LAWRENCE
LIVERMORE
NATIONAL
LABORATORY

LLNL-TR-583812

Phenomenological models of the energy dependence in fission

W. Younes

September 21, 2012

Disclaimer

This work performed under the auspices of the U.S. Department of Energy by Lawrence Livermore National Laboratory under Contract DE-AC52-07NA27344.

Phenomenological models of the energy dependence in fission

W. Younes

Lawrence Livermore National Laboratory, CA 94551

(Dated: September 14, 2012)

Abstract

We present a detailed analysis of two phenomenological models of nuclear fission, with a particular emphasis on the mechanisms used by those models to predict fragment properties from induced fission, as a function of incident energy. The formalism for both models is presented and applied to the study of fission-fragment properties (yields and energies) for the $^{235}\mathrm{U}\,(n,f)$ and $^{239}\mathrm{Pu}\,(n,f)$ reactions. The goal of this report is to lay the foundation for a hybrid approach where the advantages of the internal consistency of microscopic calculations (based on an effective interaction between protons and neutrons) can be combined with the adaptability of phenomenological models tuned to known data. This hybrid approach can in principle lead to more predictive power and accuracy than either microscopic or phenomenological models alone.

I. INTRODUCTION

The description of induced nuclear fission and of the properties of fission fragments, as a function of incident energy, remains a great challenge for both theorists and experimentalists. The current state-of-the-art microscopic theories of fission in development at LLNL and around the world can be expected to produce a more fundamental understanding of the phenomenon in the long term and, more practically, general trends of properties in the short term. But until these approaches fully mature over the coming years, wherever high-precision nuclear data are required, phenomenological models tuned to available experimental measurements, remain the necessary bridge between experiment and theory.

Phenomenological models are designed to incorporate selected features of more fundamental theories with adjustable parameters, while being generally simpler and more tractable than the theories they emulate. The free parameters in these models are tuned to experimental measurements, making them a useful tool for evaluating nuclear data. While it is not usually possible to deduce the more fundamental theory from phenomenological models, it is nevertheless possible to learn from them the general features that the fundamental theory must have in order to reproduce the data.

In this report we examine two phenomenological models, developed by Ruben et al. [1] and Schmidt et al. [8, 9], respectively, to predict fission fragment properties for induced fission as a function of incident energy. The two models differ widely in complexity, from the relatively simple model of Ruben et al., to the complex assembly of models of Schmidt et al. designed to predict a wide array of fission observables. These two models were selected because they could reproduce the experimental data, and contained readily identifiable mechanisms to treat the incident-energy dependence. The goal of this study was to extract this energy dependence and to examine if and how these models could be used with microscopic ingredients to provide reliable data wherever experiments cannot be performed. In order to gain a deeper understanding of these models and combine them with other (more microscopic) fission calculations, both phenomenological models were re-coded in full for this study. Though coding the models proved to be a daunting enterprise, it was a necessary step in order to 1) identify important aspects of the models that are never mentioned in the literature, and 2) make available the various components of the code to better understand the origin in the models of features in the observables they calculate. The formalism used

in each of the models is presented in section II. Results from calculations using the models are compared to experimental data in section III.

II. THEORY

A. Ruben et al. model

1. General philosophy

The Two-Spheroid Model (TSM) of Ruben et al. [1] is relatively simple and manages to predict reasonably well the fission-fragment excitation and kinetic energies as a function of incident energy, without a great deal of cumbersome formalism. As the name suggests, the model begins with a simple picture of two spheroidal fragments at scission. The central equations of this model stem from the minimization of the potential energy in this scission configuration, and from the conservation of energy in the fission process. The model requires shell correction energies for each fragment, and rests on a number of simplifying hypotheses (Fermi-gas model for intrinsic fragment energies, assumption of equal temperature of the fragments at scission, quadratic form of the deformation energy of the fragments).

2. Basic formalism

In the TSM, two spheroidal fragments with semi-major axis lengths D_1 and D_2, respectively, are separated by a "tip-to-tip" distance d. The Coulomb energy of the system at scission is given by

$$E_{coul} \;=\; \frac{Z_1 Z_2 e^2}{D_1 + D_2 + d} \tag{1}$$

and the deformation energy of each fragment is assumed to be quadratic in the change of radius relative to a spherical nucleus with radius R_i, where the index $i = 1, 2$ labels the fragments,

$$E_{def}^{(i)} \;=\; \alpha_i \left(D_i - R_i\right)^2$$

Note that in all that follows, we will never need quantitative values for D_i and R_i; only the fact that the $E_{def}^{(i)}$ depend quadratically on these variables is important. Neglecting the

nuclear interaction between fragments at scission, the potential energy, consisting of the sum of the Coulomb and deformation energies, is minimized with respect to the lengths D_1 and D_2, and the relation

$$E_{def}^{(i)} \;=\; \frac{E_{coul}^4}{4\alpha_i Z_1^2 Z_2^2 e^4} \tag{2}$$

is obtained. This is the first of two central equations in the model. The deformability parameter α_i for each fragment is obtained from a liquid-drop model value [3]

$$\alpha_{LDM}\left(A\right) \;=\; 2.86 - 0.0630\frac{Z^2}{A}$$

modified by shell-correction energies δW, according to the semi-empirical relation [2]

$$\alpha\left(A\right) \;=\; \alpha_{LDM}\left(A\right)\frac{K - \delta W\left(A\right)}{K + \delta W\left(A\right)} \tag{3}$$

for a fragment of mass number A and with $K = 8.0$ MeV. A temperature dependence of the shell correction energies is introduced, as described by the Bohr-Mottelson relation [17]

$$\delta W\left(A,\tau\right) \;=\; \delta W\left(A,\tau=0\right)\frac{t^2\cosh t}{\sinh^2 t} \tag{4}$$

where the dimensionless parameter t is related to the temperature τ via

$$t \;=\; \frac{2\pi^2}{\hbar\omega_{sh}}\tau$$

and $\hbar\omega_{sh} \approx 25A^{-1/3}$ is the shell-energy distance. The total excitation energy (TXE) of the fragments and their total kinetic energy (TKE) are related to the Q value of the reaction by conservation of energy

$$TKE + TXE \;=\; Q \tag{5}$$

This equation, along with Eq. (2), form two central equations in the theory. The TKE itself is the sum of the Coulomb energy at scission (Eq. (1)) and a pre-scission energy acquired in the descent from saddle to scission,

$$TKE \;=\; E_{pre} + E_{coul} \tag{6}$$

where the pre-scission energy is given by the semi-empirical formula [5, 6]

$$E_{pre} \;=\; 2.24\frac{Z_{CN}^2}{A_{CN}} - 69.5\,(\mathrm{MeV})$$

where Z_{CN} and A_{CN} are the charge and mass number, respectively, of the compound fissioning nucleus. The total excitation of each fragment is the sum of its intrinsic and deformation excitation energies,

$$E_x^{(i)} \;=\; E_{int}^{(i)} + E_{def}^{(i)} \tag{7}$$

where the assumption is made that the fragments are at the same temperature τ and that they obey a simple Fermi-gas law,

$$E_{int}^{(i)} \;=\; a_i \tau^2 \tag{8}$$

with a_i the level density parameter corrected for shell effects [4, 5]

$$a_i\left(A, E_x^{(i)}, \delta W_0\right) \;=\; \frac{A}{8}\left[1 + \frac{\delta W_0}{E_x^{(i)}}\left(1 + e^{-0.05 E_x^{(i)}}\right)\right] \tag{9}$$

and where $\delta W_0\left(A\right) \equiv \delta W\left(A, \tau = 0\right)$ is the shell correction energy at zero temperature.

Finally, the incident energy (E_n in the case of neutron-induced reactions) contributes a "heat" energy E_h to the nucleus, measured above the second saddle,

$$E_h \;=\; S_n + E_n - E_B - \Delta \tag{10}$$

where S_n is the neutron separation energy in the compound system, E_B is the barrier height, and Δ is the pairing gap above the second saddle, and with the constraint that $E_h \geq 0$. It is assumed that the total intrinsic energy of the fragments can be decomposed as the sum of this heat energy above the saddle, and the energy E_{dis} dissipated in the descent from saddle to scission,

$$E_{int}^{(1)} + E_{int}^{(2)} \;=\; E_h + E_{dis} \tag{11}$$

where E_{dis} is taken to be [6]

$$E_{dis} \;=\; 6.2\,(\mathrm{MeV})$$

for $^{235}\mathrm{U}\,(n_{th}, f)$.

3. Solution algorithm

There is an implicit recursive structure in the formalism outlined in section II A 2, tied to the two central equations (Eq. (2) and Eq. (5)) of the model. If we choose values of the

TKE for the fragments and corresponding excitation-energy ratios

$$\rho \equiv \frac{E_x^{(1)}}{E_x^{(1)} + E_x^{(2)}} = \frac{E_x^{(1)}}{TXE} \tag{12}$$

then, for a given incident energy E_n (and therefore a corresponding Q value), we can immediately deduce the values of $E_x^{(1)}$ and $E_x^{(2)}$ from the conservation of energy Eq. (5). On the other hand, given E_n, $E_x^{(1)}$, and $E_x^{(2)}$ we can deduce the TKE and ρ values starting from Eq. (2), and working through the formalism to Eq. (6). It is not immediately clear that Eqs. (2) and (5) are consistent with each other.

The ambiguity that arises from this internal consistency issue complicates the application of the formalism, but is not explicitly discussed in the literature related to this model. This difficulty is compounded by the fact that the details of the model are not always easy to find in the literature. For this reason, we have developed our own algorithm to enforce consistency between Eqs. (2) and (5) and implemented it in a Mathematica script [7].

The application of the algorithm does not involve any adjustment of parameters. It begins with initial guesses for the TKE and energy-ratios ρ of the fragments, then the formalism in section II A 2 is used to calculate new TKE values. a range of reasonable values of TKE and ρ is systematically searched, and those that provide the best agreement between initial guess and final TKE values is selected as the correct choice. The algorithm proceeds as follows:

1. Start with initial guesses for TKE and ρ for each fragment

2. Calculate the total excitation energies of the fragments from Eqs. (5) and (12),

$$\begin{aligned} E_x^{(1)} &= \rho\, TXE \\ E_x^{(2)} &= (1-\rho)\, TXE \end{aligned}$$

3. Calculate the common temperature of the fragments from Eqs. (8) and (11)

$$\tau = \sqrt{\frac{E_{int}^{(1)} + E_{int}^{(2)}}{a_1 + a_2}} = \sqrt{\frac{E_h + E_{dis}}{a_1 + a_2}}$$

   with the level density parameters a_1 and a_2 given by Eq. (9).

4. Deduce the deformation energies from Eqs. (7) and (8),

$$\begin{aligned} E_{def}^{(1)} &= E_x^{(1)} - a_1\tau^2 \\ E_{def}^{(2)} &= E_x^{(2)} - a_2\tau^2 \end{aligned}$$

5. Calculate the deformability parameters α_i using Eqs. (3) and (4)

6. Deduce the TKE from each fragment, using Eqs. (2) and (6)

$$TKE_i \;=\; E_{pre} + \left(4\alpha_i Z_1^2 Z_2^2 e^4 E_{def}^{(i)}\right)^{1/4}$$

The index i in TKE_i refers to the fact the the total kinetic energy can be calculated using the properties of either fragment. In fact, the two estimates are mathematically equivalent by virtue of Eq. (2), which implies

$$\alpha_1 E_{def}^{(1)} \;=\; \alpha_2 E_{def}^{(2)}$$

and therefore $TKE_1 = TKE_2$.

7. As a measure of consistency of the model, we calculate

$$S \;\equiv\; \left(TKE - TKE_i\right)^2$$

where $i = 1$ or 2 (see explanation in step 6).

The form of S in step 7 is designed to enforce consistency between the initial guess for TKE, and its deduced values. Therefore, the algorithm above is used to explore a range of possible value of ρ and TKE to find the set that minimizes the value of S. The need to enforce this consistency can be seen more clearly now by tracing the dependence of α_i and $E_{def}^{(i)}$ used in step 6: the deformabilities α_i depend on the temperature τ, which depends on the level density parameters a_i, which depend on the excitation energies $E_x^{(i)}$, and which are themselves related back to ρ and TKE. Likewise, the $E_{def}^{(i)}$ energies depend on the fragment excitation energies $E_x^{(i)}$, and therefore on ρ and TKE.

B. Schmidt et al. model

1. General philosophy

The general fission model (GEF) developed by Schmidt et al. [8, 9] is fairly complex and calculates a plethora of fission observables. Given the charge (Z_{CN}) and mass (A_{CN}) numbers of the fissioning nucleus, and the energy (E_n) of the incident neutron, the model calculates the following quantities:

- Yields as a function of fragment charge number
- Yields as a function of fragment neutron number (both before and after neutron emission)
- Yields as a function of fragment mass number (both before and after neutron emission)
- Independent mass-chain yields as a function of fragment mass and charge number (both before and after neutron emission)
- Spectrum of prompt gammas
- Spectrum of prompt neutrons in the center-of-mass system
- Fragment angular-momentum distribution (both before and after neutron emission)
- Relative independent isomeric yields
- Yields as a two-dimensional function of fragment mass and kinetic energy
- Neutron multiplicity distribution

The basic principle underlying the GEF model is that the features of fission yields are determined by the liquid-drop model (LDM), modified by shell corrections. These shell effects are assumed to depend on the fragments, but not on the fissioning nucleus. Thus, fission is described by three main fission modes (corresponding to valleys in the potential energy surface): the superlong (SL) mode associated with the LDM, the S1 mode for spherical heavy (A $\sim$ 134) and deformed light fragments, and the S2 mode for moderately deformed heavy (A $\sim$ 140) and moderately deformed light fragments. In addition, an S3 mode is used for very asymmetric fission. In the description of the formalism below, the modes will be designated by the index i with $i = 0$ for SL, $i = 1$ for S1, etc. In addition, the model tries to include both dynamical and quantum-mechanical effects.

Dynamical effects are introduced to take into account the evolution of the fissioning system from its initial formation to scission. It is well known, from limitations of scission-point models (see e.g., [13, 25]) that the detailed behavior of the fissioning nucleus prior to scission plays an important role in determining fission observables (e.g., the width of the fragment mass distribution). In the formalism of the model, dynamical effects are

invoked to justify the assumption that different observable quantities are "frozen out" at specific stages of the fission process. In particular, it is assumed that mass distributions are essentially determined by the time the outer saddle is reached, while charge polarization (the amount by which the charge number of the fragment differs from a simple Unchanged Charge Distribution (UCD) [14] estimate) is fixed closer to scission.

Quantum-mechanical estimates of these dynamical effects are obtained using the simplified picture of a quantum-mechanical harmonic oscillator coupled to a heat bath at finite temperature, and is used to characterize the motion (vibrations) of the nucleus perpendicular to the fission path. In practice, this quantum-mechanical picture introduce zero-point motion of the harmonic oscillator, which is used to calculate widths of fragment distributions. In addition, the "orientation pumping" mechanism [15], due to the uncertainty principle, is used in the model to account for the angular momentum of the fragments.

For the purposes of this report we will be primarily concerned with the treatment of the energy dependence of those yields in the model. The dependence of the model on incident neutron energy appears principally in three places: 1) the magnitude of the yield for each mode, 2) the width of the mass distribution for the mode, and 3) the excitation energy of the fragments, which then determines the multiplicity and energy of neutrons and gammas emitted by the fragments. We briefly describe the salient features of the energy dependence in those three aspects of the model next.

2. Energy dependence of fission mode yields

For each fission mode i, the total yield Y_i is given by the product of a constant-temperature state density and a Hill-Wheeler barrier transmission coefficient,

$$Y_i \;=\; \frac{\exp\left[E_x^{(i)}/T_{hi}^{(i)}\right]}{1+\exp\left[-E_x^{(i)}/\left(\frac{T_{hi}^{(i)}T_{lo}^{(i)}}{T_{hi}^{(i)}-T_{lo}^{(i)}}\right)\right]} \tag{13}$$

where $T_{hi}^{(i)}$ is the intrinsic temperature given (in MeV) by the empirical formula [10]

$$T_{\rm int}\left(A_{CN},\delta U^{(i)}\right) \;=\; \frac{F_{\rm red}}{A_{CN}^{2/3}}\left(17.45-0.51\delta U^{(i)}+0.51\left(\delta U^{(i)}\right)^2\right) \tag{14}$$

and where $F_{\rm red}$ is an empirical reduction factor set to 0.8 in the calculations, and $\delta U^{(i)}$ is a shell correction energy. The "effective temperature below barrier", $T_{lo}^{(i)}$ has a value of ~ 0.3

MeV for each mode i. The excitation energy $E_x^{(i)}$ for each mode is measured relative to a corresponding calculated saddle height B_i,

$$E_x^{(i)} \;=\; E_n + S_n - B_i$$

where E_n is the incident energy and S_n is the neutron separation energy in the fissioning nucleus.

3. Energy dependence of fission mode widths

For mode i, the associated potential energy is expanded to second order in the charge Z [11],

$$V^{(i)}(Z) \;=\; V^{(i)}\left(Z_c^{(i)}\right) + C^{(i)}\left(Z - Z_c^{(i)}\right)^2 \tag{15}$$

Placing the system in a heat bath of temperature T, the corresponding probability of the system having charge Z is given by the Boltzmann distribution

$$\begin{aligned} P^{(i)}(Z) \;&\propto\; e^{-V^{(i)}(Z)/T} \\ &\propto\; \exp\left[-\frac{C^{(i)}\left(Z - Z_c^{(i)}\right)^2}{T}\right] \end{aligned}$$

which is a Gaussian with variance

$$\sigma_i^2 \;=\; \frac{T}{2C^{(i)}} \tag{16}$$

This is the basic form used to calculate the widths of charge distributions for the different modes. The coefficients $C^{(i)}$ are expected to have an energy dependence for $i \neq 0$ due to the washing out of shell effects. The collective temperature T in this case is given by a fairly complicated expression which becomes roughly linear in excitation energy $E_x^{(i)}$ for $E_x^{(i)} \gg 0.7\,\mathrm{MeV}$. The coefficients $C^{(i)}$ are given an empirical energy dependence

$$C^{(i)} \;\propto\; \exp\left(-\frac{E_{\mathrm{int}}^{(i)}}{18.5}\right)$$

where $E_{\mathrm{int}}^{(i)}$ is the excitation energy $E_x^{(i)}$, reduced by a pairing energy.

4. Energy dependence of the fragment excitation energies

The excitation energy above saddle, $E_x^{(i)}$, appears as intrinsic energy of the fragments via the "energy-sorting" mechanism described in [12]. The sum of intrinsic excitation energies for the light and heavy fragments, in a form reminiscent of Eq. (11), is given by the sum of excitation energy above saddle ($E_x^{(i)}$) and a contribution from the descent from saddle to scission.

5. Solution algorithm

Without going into great detail, we list here the important steps in the execution of the GEF algorithm:

1. Calculate shell correction energies
2. Calculate fission barriers
3. Calculate excitation energies above those barriers
4. Calculate the yield magnitude for each fission mode (Eq. (13))
5. Calculate collective temperature for each fission mode (needed for the calculation of the mass distribution widths)
6. Calculate mass distribution width for each fission mode (Eq. (16))
7. Calculate deformations of fragments
8. Calculate charge-number polarization of fragments (relative to UCD estimate)
9. Calculate mass-distribution centroids using the charge polarizations obtained in the previous step
10. Calculate even-odd effect on yields
11. Calculate stiffness in polarization (needed in the calculation of charge distributions)
12. Construct pre-neutron fragment distributions using the yield magnitudes, widths, and centroids obtained in the steps above

13. Calculate excitation energy of each fragment consisting of contributions from deformation, intrinsic (via the energy-sorting mechanism [12]), and collective energy (taken as a fraction of the energy acquired in the descent from saddle to scission

14. Calculate neutron evaporation by subtracting kinetic and separation energy of each emitted neutron from remaining excitation energy, until there is insufficient energy left to emit any more neutrons

15. Construct post-neutron fragment distributions from the pre-neutron distributions and calculated emission information

III. DISCUSSION

A. Ruben et al. model

Our initial attempts to reconstruct this model based on published descriptions were not entirely successful. After many attempts we found that, in order to replicate the author's calculation, the barrier height E_B in Eq. (10) could not be taken as a constant, but had to instead depend on the fragment mass. In the end, this variable barrier height was found by assuming that the experimental mass yield is roughly given by

$$Y(A) \propto \exp\left[-\frac{E_B(A)}{\hbar\omega_b}\right] \tag{17}$$

with $\hbar\omega_b = 1$ MeV, and where the yields $Y(A)$ were taken from experiment at thermal neutron energies. Intuitively, Eq. (17) incorporates the basic feature of the Hill-Wheeler transmission coefficient whereby the yields of fragments from symmetric to very asymmetric division of the nucleus are essentially determined by excitation energy above the barrier. The effect of this variable barrier can be seen in Fig. 1 which shows the difference in TKE(A) between $E_n = 6$ MeV and thermal energies for $^{235}\mathrm{U}(n, f)$. The curve labeled "E_B from $Y(A)$", obtained using Eq. (17) is in good agreement with the original calculation by Ruben et al., in contrast to the standard calculation with constant barrier height (labeled "$E_B = \mathrm{const}$"). Both the Ruben et al. and present calculations using a variable barrier are in good agreement with the experimental data. Figs. 2 and 3 show similarly good agreement between experimental data and calculations for $E_n = 1$ and 4 MeV, respectively. Thus the

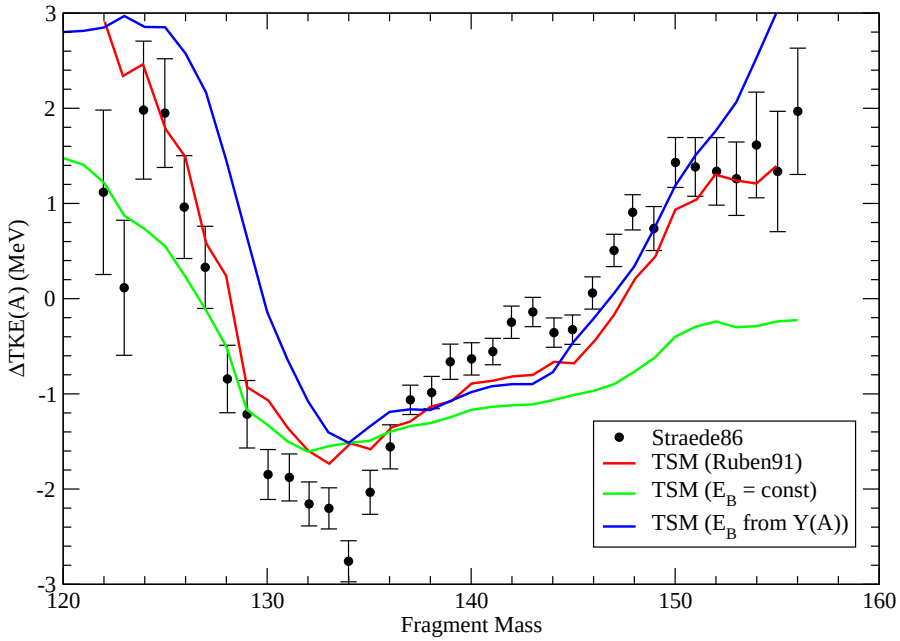

Figure 1: Difference between fragment kinetic energies at $E_n = 6$ MeV and thermal. Experimental data [20] are compared to the two-shell model (TSM) of Ruben et al. [1]. See text for details.

trends in TKE as a function of E_n are well reproduced by the washing out of shell effects according to Eq. (4).

B. Schmidt et al. model

The GEF code uses a Monte-Carlo approach to generate the pre- and post-neutron fragment distributions. We have reprogrammed this code as a Mathematica [7] script using deterministic, analytical formulas instead, in order to better understand the details of the formalism. Having analyzed the code in detail, we proceeded to calculate post-neutron mass distributions and compared them to evaluated chain yields [16]. The comparisons between GEF and experiment are shown in Fig. 4 for ^{235}U (n, f), and Figs 5 and 6 for ^{239}Pu (n, f). In general the agreement between experiment and theory is fairly good, with discrepancies of at most $\approx 25\%$.

The results in Figs. 4-6 are certainly very encouraging, but they only showcase the

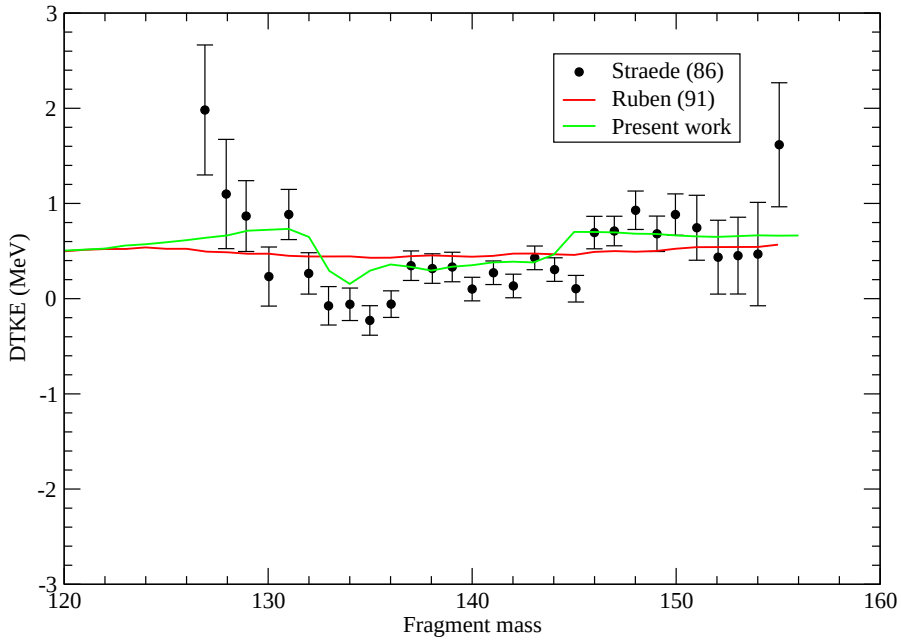

Figure 2: Same as Fig. 1 for E_n= 1 MeV.

model's ability to reproduce relative quantities (since the total yield, integrated over all fragment masses, must equal 200% by convention). In Figs. 7 and 8 we examine the model's ability to predict absolute quantities. In Fig. 7, we show the average neutron multiplicity for the ^{235}U$\,(n,f)$ and ^{239}Pu$\,(n,f)$ reactions, as a function of incident energy, compared to the corresponding ENDF/B-VII evaluation. In both cases, the GEF calculation overestimates the evaluated curve by a small but noticeable amount. This result may indicate an overestimate of the excitation energy of the fragments, which is further supported by the kinetic-energy plots in Fig. 8.

Fig. 8 compares the GEF calculations of kinetic energy relative to thermal-neutron induced fission to the TSM model results displayed in Figs. 1, 2, and 3. These curves were obtained from the two-dimensional yields as a function of fragment mass and kinetic energy produced by the GEF code. The GEF calculations clearly show that an excessive amount of the energy contributed by the incident neutron is dissipated into excitation energy of the fragments, to the detriment of their kinetic energies. In fact, the GEF curves showing the TKE of the fragments, relative to the TKE due to thermal-induced fission, underestimates

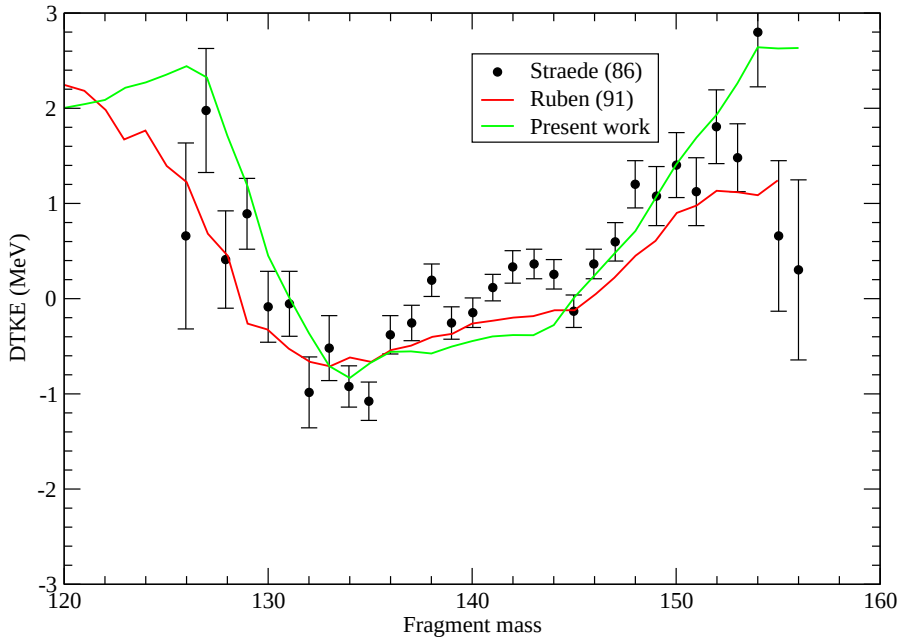

Figure 3: Same as Fig. 1 for E_n= 4 MeV.

the data and TSM calculations by up to several MeV's, with the worst discrepancies near very symmetric and very asymmetric fission configurations.

IV. CONCLUSION

We have studied the treatment of the energy dependence of fission in two separate phenomenological approaches with very different levels of internal complexity. The two models, by Ruben et al. and Schmidt et al. respectively, rely on a standard washing-out of shell effects with increasing temperature to reproduce experimental trends in fragment yields and energies as a function of incident neutron energy. The Ruben et al. model provides good qualitative agreement with kinetic-energy trends for ^{235}U (n, f), while the Schmidt et al. model gives a 25% or better agreement with measured fission chain yields for ^{235}U (n, f) and ^{239}Pu (n, f), with less satisfactory results for the kinetic energies of the fragments. The contrast between the complexity and performance of the two models is illuminating in itself. At one end of the spectrum, the GEF model of Schmidt et al. represents one extreme of

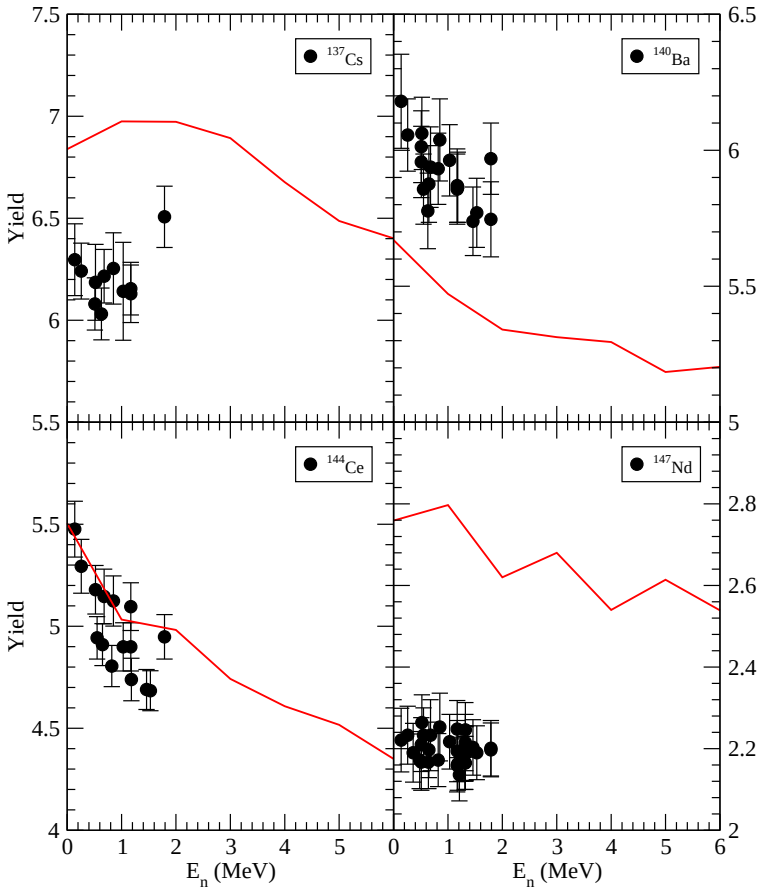

Figure 4: Experimental chain yields for $^{235}\mathrm{U}\,(n,f)$ [16] compared to calculations using the GEF model.

sophistication for phenomenological models and is able to predict a vast array of experimental observables for many nuclei, yet it is outperformed in the prediction of the total kinetic energy of the fragments by the much simpler TSM model of Ruben et al. There are several observations that can be drawn from this contrast. First, fission is an extremely difficult phenomenon to describe, and it should come as no surprise that even the most sophisticated models can produce satisfactory results for some observables while encountering greater difficulty with others. In general, the $\sim 25\%$ agreement between model and experiment appears to be a reasonable fiducial level of agreement that can be expected for modern models and theories of fission. Second, in light of the complexity of the fission problem, internal

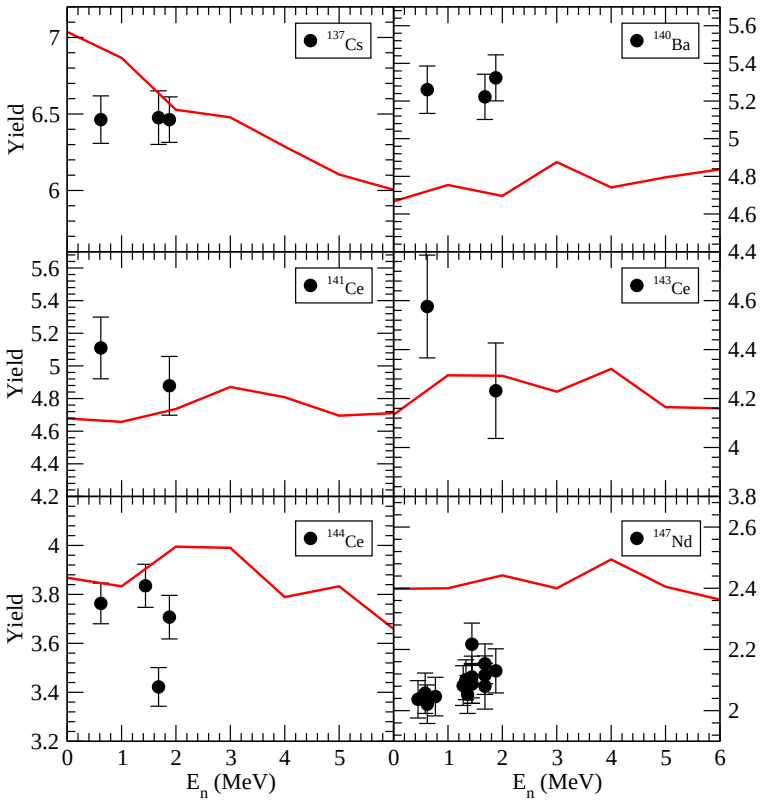

Figure 5: Experimental chain yields for $^{239}\mathrm{Pu}\,(n,f)$ [16] compared to calculations using the GEF model.

consistency of the models becomes of paramount importance. Thus, the true test of the predictive power of a fission model should not be limited to its ability to reproduce known experimental results, but must include a close examination of internal consistency in the inner workings of the model. All fission models are necessarily built on approximations and hypotheses, what is important is whether those approximations and hypotheses, validated in systems where experimental data are available, still hold where there are no available measurements.

In each of the phenomenological models we have studied, microscopic calculations, which are not tuned to the fission observables of interest, could be used to replace many of the

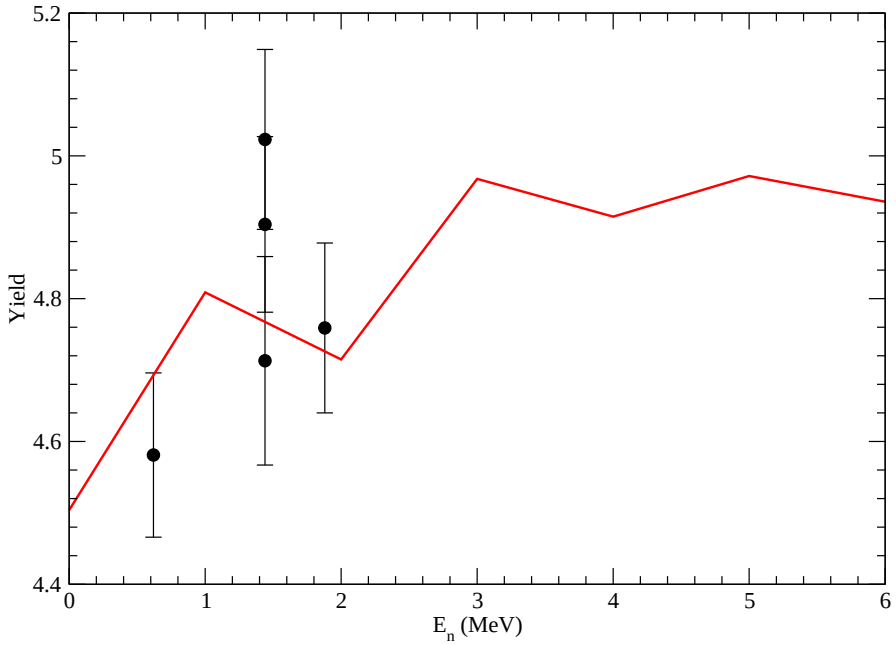

Figure 6: Same as Fig. (5), but for the ^{95}Zr fission product.

simplifying assumptions with self-consistent calculations. In the Ruben et al. model, the spheroidal fragments can be replaced by a more realistic calculation of the nucleus at scission [26] and the assumption of equal temperature of the fragments can be fully investigated using temperature-dependent Hartree-Fock-Bogoliubov calculations. Deformation and internal excitation energies can also be provided by microscopic calculations. In the Schmidt et al. approach, the calculation of the mass yield strength and width is currently being explored at LLNL using a fully microscopic theory wherein a wave packet over microscopic nuclear states evolves to scission according to the laws of quantum mechanics.

Most usefully, in this analysis we have pinpointed the mechanisms by which the energy dependence is introduced into these phenomenological models (Eqs. (4) for Ruben et al., and (13) and (16) for Schmidt et al), which rely essentially on the introduction of temperature. Temperature in these phenomenological models is used to mimic the effects of exchanges of energy between different degrees of freedom during the dynamical evolution of the nucleus to scission. In contrast to the phenomenological models considered here, the dynamic exchange of energy between degrees of freedom is explicitly calculated in the microscopic approaches to

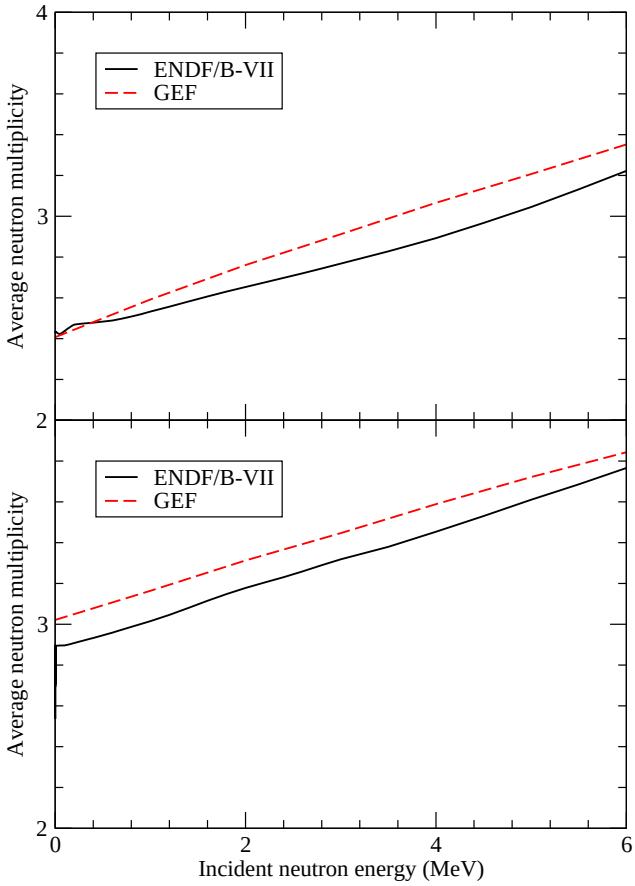

Figure 7: Average neutron multiplicity as a function of incident neutron energy calculated by the GEF model and compared to the ENDF/B-VII evaluations for ^{235}U(n, f) [21] (top panel) and ^{239}Pu(n, f) [22] (bottom panel).

low-energy fission in development at LLNL. As we continue to develop this fully microscopic theory of induced fission and of its dependence on incident energy, we will be in a position to improve the ingredients in the phenomenological approaches in order to provide precise and reliable results for nuclear data evaluations.

The author is grateful to D. Gogny for a critical reading of this report, and for many useful suggestions. This work was performed under the auspices of the US Department of Energy

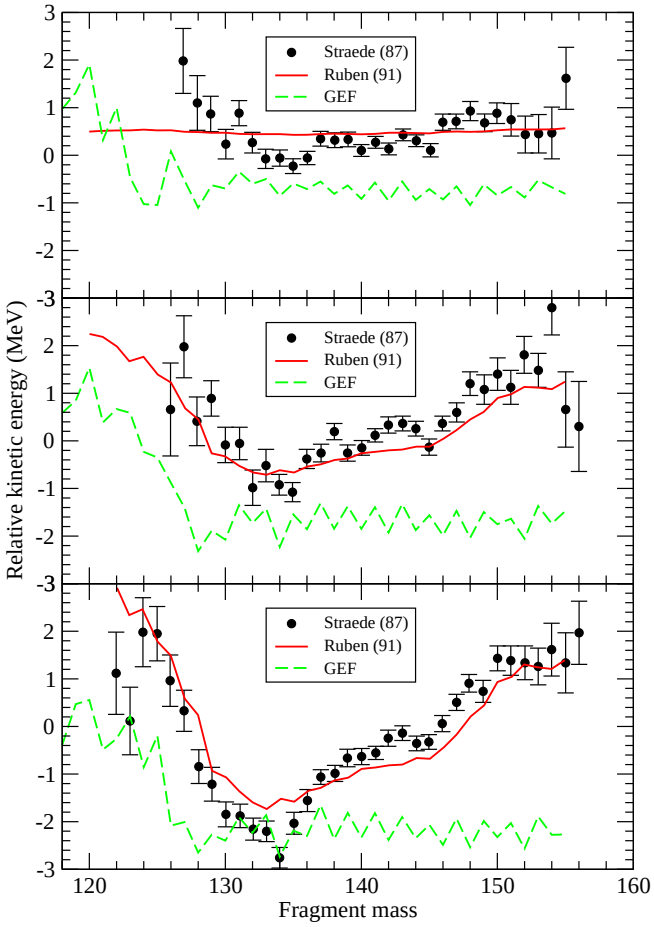

Figure 8: Kinetic energy relative to the thermal-fission kinetic energy, plotted as a function of fragment mass for $E_n = 1$ MeV (top panel), 4 MeV (middle panel) and 6 Mev (bottom panel). The solid points are data taken from [20], the solid red lines are the calculations of Ruben et al. [1], and the dashed green line is the result extracted from the GEF code [9].

by the Lawrence Livermore National Laboratory under Contract DE-AC52-07NA27344.

---

[1] A. Ruben, H. Märten, and D. Seeliger, Zeit. Phys. A 338, 67 (1991).

[2] M. Kildir and N. K. Aras, Phys. Rev. C 25, 365 (1982).

[3] J. Terrell, Proc. IAEA Symp. on Physics and Chemistry of Fission, Salzburg, 1965 (IAEA, Vienna, 1965), vol II, 3.

[4] A. V. Ignatyuk, G. N. Smirenkin, and A. S. Tischin, Yad. Fiz., 21, 485 (1975).

[5] H. Märten, A. Ruben, and D. Seeliger, Nucl. Sci. and Eng. 109, 120 (1991).

[6] F. Gönnenwein, J. P. Bocquet, and R. Brissot, Proc. 17th Int. Symp. Nucl. Phys., Gaussig, GDR, 1987, 129 (ZfK-646).

[7] Wolfram Research, Inc., "Mathematica Edition: Version 7.0", Wolfram Research, Inc. Champaign, IL 2008.

[8] K.-H. Schmidt and B. Jurado, JEF/DOC 1423 (2011).

[9] GEF code and documentation available for download at http://www.cenbg.in2p3.fr/-GEF-

[10] T. Von Egidy and D. Bucurescu, Phys. Rev. C 72, 044311 (2005).

[11] F. Gönnenwein, in Proceedings of the XVIIIth International Symposium on Nuclear Physics, Gaussig 1988, p. 12 (ZfK-732).

[12] K.-H. Schmidt and B. Jurado, Phys. Rev. Lett. 104, 212501 (2010).

[13] B. D. Wilkins, E. P. Steinberg, and R. R. Chasman, Phys. Rev. C 14, 1832 (1976).

[14] A. C. Wahl, R. L. Ferguson, D. R. Nethaway, D. E. Troutner, and K. Wolfsberg, Phys. Rev. 126, 1112 (1962).

[15] L. Bonneau, P. Quentin, I. N. Mikhailov, Phys. Rev. C 75, 064313 (2007).

[16] Chadwick et al. At. Data and Nucl. Data Sheets 111 (2011).

[17] A. Bohr and B. R. Mottelson, Nuclear Structure, vol II, New York: Benjamin 1975.

[18] P. Lichtner, D. Drechsel, J. Maruhn, and W. Greiner, Phys. Lett. B 45, 175 (1973).

[19] J. Maruhn and W. Greiner, Phys. Rev. Lett. 32, 548 (1974).

[20] Ch. Straede, C. Butdtz-Jørgensen, and H.-H. Knitter, Nucl. Phys. A462, 85 (1987).

[21] P. G. Young, M. B. Chadwick, R. E. MacFarlane, W. B. Wilson, D. G. Madland, P. Talou, T. Kawano, L. C. Leal, H. Derrien, N. M. Larson, R. Q. Wright, D. A. Brown, J. Pruet, ENDF/B-VII evaluation, MAT # 9228, Revision Dec 2006; data retrieved from the ENDF database (9/10/12).

[22] P. G. Young, M. B. Chadwick, R. E. MacFarlane, W. B. Wilson, D. G. Madland, P. Talou, T. Kawano, H. Derrien, G. de Saussure, T. Nakawa, D. A. Brown, J. Pruet, ENDF/B-VII evaluation, MAT # 9437, Revision Dec 2006; data retrieved from the ENDF database (9/10/12).

[23] Code FRHFB developed by W. Younes and D. Gogny.

[24] J. Libert, M. Girod, and J.-P. Delaroche, Phys. Rev. C 60, 054301 (1999).

[25] H. Goutte, J.-F. Berger, P. Casoli, and D. Gogny, Phys. Rev. 71, 024316 (2005).

[26] W. Younes and D. Gogny, Phys. Rev. Lett. 107, 132501 (2011).